Springer

KSME

Journal of Mechanical Science and Technology 29 (10) (2015) 4239~4246
www.springerlink.com/content/1738-494x(Print)/1976-3824(Online)
DOI 10.1007/s12206-015-0920-5

Effects of fluid thermophysical properties on cavitating flows †

Tairan Chen, Biao Huang*, Guoyu Wang and Kun Wang

School of Mechanical and Vehicular Engineering, Beijing Institute of Technology, Beijing, 100081, China

(Manuscript Received February 15, 2015; Revised May 3, 2015; Accepted May 13, 2015)

Abstract

We studied the thermo-fluid cavitating flows and evaluated the effects of physical properties on cavitation behaviors. The thermo-fluid (including liquid nitrogen, liquid hydrogen and hot water) cavitating flows around a 2D hydrofoil were numerically investigated. The Favre-averaged Navier-Stokes equations with the enthalpy-based energy equation, transport equation-based cavitation model, and the *k-ω* SST turbulence model were applied. The thermodynamic parameter $\sum$, defined as $\sum = (\rho_v^2 L^2)/(\rho_l^2 C_v T_\infty \sqrt{\varepsilon_l})$ was used to assess the thermodynamic effects on cavitating flows. The results manifest that the thermal energy solution case yields a substantially shorter and mushier cavity attached on the hydrofoil due to the thermodynamic effects, which shows better agreement with the experimental data. The temperature drop inside the cavity decreases the local saturated vapor pressure and hence increases the local cavitation number; it could delay or suppress the occurrence and development of the cavitation behavior. The thermodynamic effects can be evaluated by thermophysical properties under the same free-stream conditions; the thermodynamic parameter $\sum$ is shown to be critical in accurately predicting the thermodynamic effects on cavitating flows. The surrogate-based global sensitivity analysis of liquid nitrogen cavitating flow suggests that ρ_v, C_l *and* L could significantly influence temperature drop and cavity structure in the existing numerical framework, while ρ_v plays the dominant role on temperature drop when properties vary with changing temperature. The liquid viscosity μ_l slightly affects the flow structure but hardly affects the temperature distribution.

Keywords: Cavitating flows; Thermo-fluid; Thermophysical properties; Sensitivity assessment; CFD

1. Introduction

Cavitation is a phase-change phenomenon that occurs in liquids when the local static pressure drops below the saturated vapor pressure of liquids; this phenomenon is usually assumed to be an isothermal process [1-7]. However, the isothermal hypothesis is no longer valid in cryogenic fluids cavitating flows for their temperature change and thermo-sensitive properties. Cryogenic fluids such as liquid hydrogen, liquid oxygen, liquid nitrogen and liquid helium are used in a variety of fields, including as propellants for rocket engines and other aerospace equipment, refrigerants for superconducting equipment. high energy physics accelerators and fusion reactors. The characteristic features of cryogenic cavitation behavior, such as strong thermodynamic effects, large variation in physical quantities and easy transition to cavitation state, have been pointed out in a number of reports [8-11].

The influence of thermodynamic effects on cavitation behavior was numerically and experimentally investigated as early as 1956 [12]. Thermodynamic effects on thermo-fluid cavitating flows give rise to obvious temperature drop ΔT, and then the change of temperature affects material thermophysical properties. To quantify the thermodynamic effects, a nominal temperature drop ΔT^* and the ratio between the actual temperature drop ΔT and ΔT^*, known as the *B*-factor, have been introduced as follows [13]:

$$\rho_v V_v L = \rho_l V_l C_l \Delta T \,, \tag{1}$$

$$B = \frac{V_v}{V_l} = \frac{\Delta T}{\Delta T^*}, \quad \Delta T^* = \frac{L}{C_l}\frac{\rho_v}{\rho_l} \,. \tag{2}$$

Eq. (1) is based on a simple heat balance between two phases, where L is the latent heat of vaporization, C_l is the liquid heat capacity, ρ_v is the vapor density, and ρ_l is the liquid density. *B*-factor is defined as the volume ratio between vapor and liquid phase (V_v/V_l); in order to maintain comparable cavity size (keep *B*-factor as a constant), there will be obvious actual temperature drop ΔT due to the stronger heat transfer involved for cryogenic liquids (larger nominal temperature drop ΔT^*) [14, 15]. It clearly demonstrates that the isothermal assumption, which is often used for room temperature water, is inappropriate for cryogenic cavitation behavior. Some thermophysical properties and the nominal temperature drop ΔT^* of liquid hydrogen, liquid nitrogen, and water are listed in Table 1. ΔT^* is approximately 100 times higher for liquid hy-

*Corresponding author. Tel.: +86 10 68912395, Fax.: +86 10 68912395
E-mail address: huangbiao@bit.edu.cn
† Recommended by Associate Editor Shin Hyung Lee

Table 1. Variation of thermophysical properties for liquid hydrogen, liquid nitrogen, and water on saturation curves [16].

	H_2 22.8K	N_2 83.06K	H_2O 298K	H_2O 348K	H_2O 437K
T_c (K)	33	126	647	647	647
p_v (kPa)	194.7	188.9	3.1	38.4	681.2
C_l (kJ kg^{-1} K^{-1})	11.33	2.08	4.18	4.19	4.35
C_v (kJ kg^{-1} K^{-1})	13.33	1.17	1.91	2.00	2.53
L (kJ kg^{-1})	433	191	2442	2321	2069
Density ratio R	28	95	43575	4049	253
ΔT^* (K)	1.37	0.97	0.01	0.14	1.89

drogen than for room temperature water, but it becomes higher than liquid hydrogen when water temperature is 437K, which suggests that a large temperature drop may occur in hot water cavitating flow just as in cryogenic liquids. So-called thermo-fluid means fluid with thermo-sensible properties, including cryogenic liquids, hot water, perfluorinated ketone, e.g.

To better investigate cryogenic cavitating flows, Hord [17, 18] conducted comprehensive experiments on cryogenic cavitation with liquid nitrogen and liquid hydrogen. Temperature and pressure data were measured at five locations in the cavitating region, which have been commonly employed for numerical validation for thermodynamic effects on cavitation [14, 15, 19, 20-23, 30, 31, 33, 34]. Recently, Zhang et al. [20] demonstrated that the full cavitation model provides a satisfactory robustness and reasonable prediction capability for simulating the cavitating flow in liquid hydrogen over different objects. Utturkar et al. [14] developed a mushy Interfacial dynamic-based (IDM) cavitation model to simulate the cryogenic cavitation behavior over two geometries (2D hydrofoil and axisymmetric ogive). Huang et al. [21] validated a thermodynamic cavitation model based on bubble dynamic equation and calibrated the parameters of the cavitation model for liquid hydrogen cavitating flows. Zhu et al. [22] developed an effective computational approach to simulate cryogenic cavitation by implementing the Schnerr-Sauer cavitation model, coupled with the energy equation. Zhang et al. [23] developed a thermodynamic cavitation model to simulate the cavitating water flow in a wide temperature range; it is seen that the thermodynamic effects of cavitation, vapor depression and temperature depression are much more predominant in high temperature water compared with those in room temperature water. Tseng and Shyy [24] conducted global sensitivity analysis to assess the role of model parameters of a transport-based cryogenic model. The cavitation model parameters, which seem to be dependent on the fluid type in the Merkle model are calibrated for liquid nitrogen and hydrogen with numerical experimentation. Murakami et al. [25] conducted a series of experiments of superfluid helium (He II) cavitating flows; the experimental results were examined in particular focusing on the thermodynamic effects by referring to the thermodynamic parameter $\sum$ introduced by Brennen [8]. Yoshida et al. [26] used a non-dimensional thermodynamic parameter $\sum^*$ which is conducted by Franc [13] to evaluate the thermodynamic effects on a nitrogen inducer; it indicated that the intensity of thermodynamic effects decreases with decreasing temperature.

Although the thermodynamic effects on cryogenic liquid cavitating flows have received much attention in past years, the effects of material thermophysical properties on cavitation behaviors are still not well understood.

Based on the numerical framework coupled with the energy equation, the present works are to study the thermo-fluid cavitating flows and to evaluate the effects of physical properties on cavitation behaviors.

2. Governing equations and numerical approaches

2.1 Governing equations

The governing equations for thermo-fluid cavitation behaviors under the homogeneous multiphase flows strategy consist of the conservative form of the Favre-averaged Navier-Stokes equations, the enthalpy-based energy equation, the turbulence closure, and a transport equation for the liquid volume fraction. The continuity, momentum, enthalpy, and cavitation model equations are given below in the Cartesian coordinates. All computations presented below are based on the steady-state equations.

$$\frac{\partial \rho_m}{\partial t}+\frac{\partial(\rho_m U_j)}{\partial x_j}=0\,, \tag{3}$$

$$\frac{\partial(\rho_m U_i)}{\partial t}+\frac{\partial(\rho_m U_i U_j)}{\partial x_j}= -\frac{\partial p}{\partial x_i}+\frac{\partial}{\partial x_j}[(\mu_m+\mu_{tur})(\frac{\partial U_i}{\partial x_j}+\frac{\partial U_j}{\partial x_i}-\frac{2}{3}\frac{\partial U_k}{\partial x_k}\delta_{ij})] \tag{4}$$

$$\frac{\partial}{\partial t}\left(\rho_m(h+f_v L)\right)+\frac{\partial}{\partial x_j}\left(\rho_m U_j(h+f_v L)\right) =\frac{\partial}{\partial x_j}\left[\left(\frac{\mu_m}{\mathrm{Pr}_{lam}}+\frac{\mu_{tur}}{\mathrm{Pr}_{tur}}\right)\frac{\partial h}{\partial x_j}\right] \tag{5}$$

$$\frac{\partial \rho_l \alpha_l}{\partial t}+\frac{\partial(\rho_l \alpha_l U_j)}{\partial x_j}=\dot{m}^+ +\dot{m}^-\,, \tag{6}$$

$$\rho_m=\rho_l\alpha_l+\rho_v\alpha_v\,, \tag{7}$$

$$\mu_m=\mu_l\alpha_l+\mu_v\alpha_v\,, \tag{8}$$

where ρ_m is the mixture density, ρ_l and ρ_v are the liquid and vapor density, respectively, α_l and α_v are the liquid fraction and the vapor fraction, respectively, U is the velocity, p is the pressure, μ_m is the mixture laminar viscosity, μ_l and μ_v are the liquid and vapor dynamic viscosities, respectively, and μ_{tur} is the turbulent viscosity, f is the mass volume fraction, L is the latent heat, h is the enthalpy, Pr_{tur} and Pr_{lam} are the turbulent and laminar Prandtl number, respectively, C is specific heat capacity at constant pressure. The subscripts (i, j, k) denote the

directions of the Cartesian coordinates. The source term $\dot{m}^+$ and the sink term $\dot{m}^-$ in Eq. (6) represent the condensation and evaporation rates, respectively.

The computations in this paper are performed by using the commercial CFD code CFX to solve the Navier-Stokes equations. The *k-ω* SST (shear stress transport) turbulence model is used, which combines the advantages of the original *k-ε* and *k-ω* models by using the *k-ω* model near the wall, and the *k-ε* model away from the wall [27].

2.2 Transport equation-based cavitation model

The source term $\dot{m}^+$, and the sink term $\dot{m}^-$, in Eq. (6) represent the condensation and evaporation rates. The liquid-vapor evaporation and condensation rates for the present transport equation-based cavitation model [14, 24, 28-31] are respectively shown as the following:

$$\dot{m}^- = \frac{C_{dest}\alpha_l}{t_\infty}\frac{\rho_l}{\rho_v}\frac{MIN(p-p_v(T),0)}{(0.5\rho_l U_\infty^2)} \tag{9}$$

$$\dot{m}^+ = \frac{C_{prod}(1-\alpha_l)}{t_\infty}\frac{MAX(p-p_v(T),0)}{(0.5\rho_l U_\infty^2)}. \tag{10}$$

C_{dest} and C_{prod} are two empirical coefficients, which are $C_{des}=3.8$ and $C_{prod}=20$ via numerical experimentation [30, 31], U_∞ is the reference velocity scale, and t_∞ is the reference time scale, which is the characteristic length scale L_c divided by the reference velocity scale $U_\infty(t_\infty = L_c/U_\infty)$. α_l is liquid volume fraction. p_v is the phase-change threshold pressure.

The experimental investigations demonstrated significant effect of turbulence on cavitating flows, which is defined as p_{tur}, k is local turbulence energy. p_v is set to be higher than the local saturation pressure $p_v(T)$ as follows [32]:

$$p_v = (p_v(T) + p_{tur}/2), \quad p_{tur} = 0.39\rho_m k. \tag{11}$$

2.3 Numerical setup and description

The numerical predictions in the present study are compared with the experimental measurements around a hydrofoil in liquid nitrogen cavitating flow investigated by Hord [17]. The computational domain and boundary conditions are shown in Fig. 1. A no-slip wall boundary condition is imposed on the hydrofoil surface, and no-slip symmetry conditions are imposed on the side boundaries, the inlet velocity is set based on the experimental data, and the outlet pressure is set to vary according to the cavitation number, defined as $\sigma_\infty = (p_\infty - p_v(T_\infty))/(0.5\rho_l U_\infty^2)$. For thermo-fluid cavitation simulation, the main temperature-dependent properties are updated from a comprehensive data base [16]. The 2D fluid mesh, which is the same as Huang [21] and Shi [31], is composed of 19000 elements with 220 structured elements across the foil boundary layer; it is selected to ensure $y^+ = yu_\tau/\nu_m = 1$, where y is the thickness of the first cell from the foil surface, and u_τ is the wall frictional velocity.

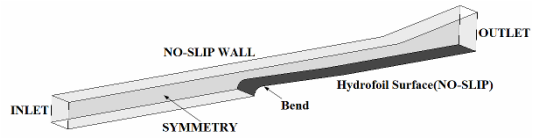

Fig. 1. 2D computation domain and boundary conditions.

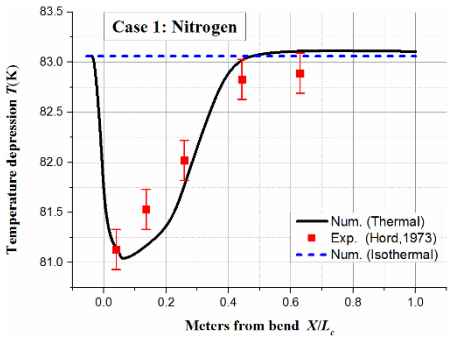

(a) Temperature depression along the surface

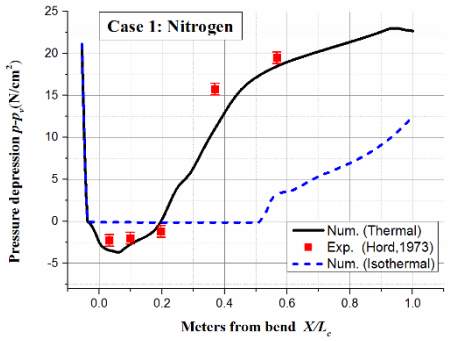

(b) Pressure depression along the surface

Fig. 2. Comparisons between results with the thermal energy and the isothermal solution for case 1.

3. Results and discussion

3.1 Characteristics of thermo-fluid cavitation behavior

Using the numerical method mentioned above, the liquid nitrogen cavitating flow which shows quintessential characteristics of thermo-fluid cavitation behaviors [14, 22, 30, 31, 33, 34] is calculated; it is selected to aid the thermo-fluid characteristic and numerical model validation. Case 1 is Case 290C in Ref. [17]; the numerical results predicted with thermal energy and isothermal solutions are illustrated in Fig. 2. Significant differences between these two kinds of solution are observed; the numerical model with thermal energy solution can consistently capture the main features of both temperature and pressure profiles. The predicted temperature and pressure distribution around the hydrofoil is steeper under the thermal energy solution than that under the isothermal solution, which shows better agreement with the experimental data. The temperature drop (evaporative cooling) inside the cavity in Fig.

2(a) decreases the local saturated vapor pressure and hence increases the local cavitation number, resulting in a smaller cavity. A slight temperature rise can also be found above the reference fluid temperature at the rear of the cavity, which is attributed to the release of latent heat during the condensation process. As temperature inside the cavity decreases, the local saturated vapor pressure decreases, which is why the value of p-$p_v(T_\infty)$ is below zero in the cavity region as well as the pressure inside the cavity is steeper under the thermal energy condition than that under the isothermal condition in Fig. 2(b). Overall, temperature change in thermo-fluid cavitating flow leads to the variations of material physical properties, and then the pressure fields and cavity structures are significantly changed.

As previously introduced, the nominal temperature drop ΔT^*, which is based on a simple heat balance between two phases, could directly predict temperature drop in thermo-fluid cavitating flows; however, the reference temperature T_∞ and the heat diffusion are not taken into consideration, and hence it is difficult to compare the thermodynamic effects on different substances.

To discuss the thermodynamic effects accurately, the thermodynamic parameter $\sum$ [8] defined by

$$\sum = \frac{\rho_v^2 L^2}{\rho_l^2 C_l T_\infty \sqrt{\varepsilon_l}}, \quad \varepsilon_l = \frac{K_l}{\rho_l C_l}, \tag{12}$$

is introduced. Based on Rayleigh-Plesset equation of single spherical bubble dynamic, considering the energy balance equation and the heat diffusion equation [8], the thermodynamic parameter $\sum$ (whose units are m/s$^{3/2}$) is used to calculate temperature change with varying bubble diameter and is crucially important in determining the bubble dynamic behavior.

Here, ρ is the density, L is the latent heat of vaporization, C is the specific heat at constant pressure, ε is the thermal diffusivity (works in unsteady heat transfer process) and K is the thermal conductivity. The suffixes v and l are indicative of vapor and liquid phase. The density ratio between liquid phase and vapor phase affects cavity size; to keep the same cavity size, smaller density ratio means more vaporization. Meanwhile, larger latent heat L and smaller specific heat C_v lead to larger temperature drop ΔT (thermodynamic parameter $\sum$ also becomes larger) during phase change.

The variation of the parameter $\sum$ for liquid nitrogen, liquid hydrogen and water is illustrated in Fig. 3 as a function of reduced temperature T/T_c (T_c is the critical temperature). The value of $\sum$ increases with increasing temperature because it is determined by temperature-dependent material properties, which suggests stronger thermodynamic effects under the same free-stream conditions. These parameters are relatively large for hydrogen and nitrogen through the whole temperature (from the triple point to the critical point); meanwhile, the value for the hydrogen is larger than the nitrogen, which means the thermodynamic effect in liquid hydrogen is stronger [14, 19, 22, 31, 34]. As to water, the value of $\sum$ is

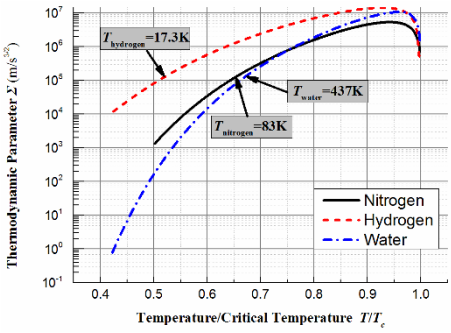

Fig. 3. The thermodynamic parameter $\sum$ for liquid nitrogen, liquid hydrogen and water as a function of reduced temperature T/Tc.

significantly small when the temperature is low, which is why the thermodynamic effects could be ignored in room temperature water. However, the slope of $\sum$ for the water is large; the magnitude of the value for water is almost the same as nitrogen when temperature is approximately 350K. It could be observed that the $\sum$ value for water at 437K, nitrogen at 83K (Case 1) and hydrogen at 17.4K are almost the same, which suggests that the intensity of thermodynamic effects of these three substances are almost the same, namely, strong thermodynamic effects could also appear in hot water cavitating flow as in cryogenic fluids.

Cavitating flows of these fluids are calculated; Table 2 summarizes the calculation conditions and results of these test cases. As previously discussed, case 1 is the liquid nitrogen cavitating flow (Case 290C in Ref. [17]), it shows quintessential characteristics of thermo-fluid cavitation behaviors. Case 2 and case 3 are applied to compare thermodynamic effects on different substances; the same σ_∞ and R_e and the similar $\sum$ are kept in these two cases.

It is observed in Fig. 4 that cavity size with thermal energy solution is decreased because the temperature drop (evaporative cooling) inside the cavity decreases the local vapor pressure and vapor/liquid density ratio, and hence increases the local cavitation number, resulting in a weaker cavitation intensity; that is how thermodynamics affects the cavitation characteristics of thermo-fluids.

The $\sum$ values for case 2 (hydrogen) and case 3 (water) are similar to case 1 (nitrogen), and the main features of each case with different solution are basically similar. It is observed that thermodynamic effects also play a significant role in hot water cavitating flow just as in cryogenic fluids. As Table 2 lists, temperature drop in water is approximately 4.10K (which is about 2.03K in nitrogen, 0.70K in hydrogen), it is difficult to assess temperature drop in different fluids, because the triple point and the critical point of substances are significantly different, and then non-dimensional $\Delta T_{max}/(T_c$-$T_\infty)$, which considers the critical temperature and the free-stream temperature is considered and the results are listed in Table 2. The order of magnitude of $\Delta T_{max}/(T_c$-$T_\infty)$ in these three cases is approximately the same, which indicates that the intensity of thermodynamic effects on different fluids is similar. The thermody-

Table 2. The calculation conditions and results for the thermo-fluids.

Case	Freestream temperature T_∞/K	Freestream velocity U_∞/(m·s^{-1})	Cavitation number σ_∞	Reynolds number R_e	Thermal parameter $\sum$/(m·s$^{-3/2}$)	Temperature drop ΔT_{max}/K	$\frac{\Delta T_{max}}{T_c - T_\infty}$/%
Case 1: Nitrogen	83.06	23.90	1.70	9.1*10^6	143492.7	2.03	4.73
Case 2: Hydrogen	17.30	33.64	1.70	9.1*10^6	140305.6	0.70	4.46
Case 3: Water	437.00	26.40	1.70	9.1*10^6	146923.5	4.10	1.95

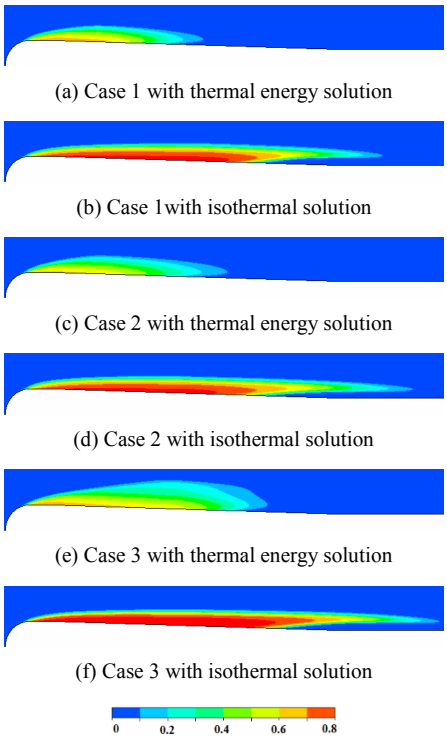

(a) Case 1 with thermal energy solution

(b) Case 1with isothermal solution

(c) Case 2 with thermal energy solution

(d) Case 2 with isothermal solution

(e) Case 3 with thermal energy solution

(f) Case 3 with isothermal solution

Fig. 4. Comparisons for vapor volume fraction of different cases.

namic effects of cavitating flow are determined by thermophysical properties rather than fluid types under the same freestream conditions. It indicates that thermodynamic parameter $\sum$ is critical in accurately predicting the intensity of thermodynamic effects on thermo-fluid cavitating flows, and the thermodynamic effects can be evaluated by physical properties.

3.2 Assessment of the thermophysical properties

As previously discussed, thermo-sensible physical properties and temperature drop significantly influence the mass transfer process and flow structure in thermo-fluid cavitating flows. In this section, the properties of liquid nitrogen are characterized by surrogate-based global sensitivity analysis and then the weights of each variable are evaluated.

Thermophysical properties like liquid density ρ_l and saturated vapor pressure p_v could directly impact the σ_∞, and hence they are kept constant. Thermal diffusivity α is not taken into consideration because of the steady computation. Since temperature change is small in cavitating flow, thermal conductivity K is ignored. Then properties like vapor viscosity and surface tension, which have little influence on thermodynamic effects, are ignored either. The vapor density ρ_v affects the mass transfer process [5], liquid and vapor heat capacity C_l and C_v influence the temperature change, and latent heat L determines the energy of release during the phase change. Therefore, these four thermophysical material properties, ρ_v, C_l, C_v, L, are chosen as design variables primarily, keeping Reynolds number R_e and cavitation number σ_∞ constant for the given case 1. Secondly, the liquid viscosity, which influences the flow structure is taken into consideration [35]. To keep the computational expense reasonable, the material properties are perturbed within ±10% of the value assuming from the NIST database [16]; as listed range 1 in Table 4, it is equal for them to influence the objective. The performance of the cavitation dynamics is characterized by predicted cavity length and the maximum temperature drop. Based on case 1, the responses are evaluated by using CFD simulations at 70 data points selected via face-centered cubic composite design (FCCD, [36]) and Latin hypercube sampling (LHS [37]) experimental designs. The polynomial response surface model (PRS, [36]), Kriging model (KRG [38]), radial basis neural network (RBNN, [39]), and a weighted average surrogate model (WAS [40]) are constructed for approximation of response. The smallest root mean square of PRESS (PRESS is the predicted residual sum of square) of different surrogate models is listed in Table 3. It is observed that the WAS model has the best performance, while KRG model has the worst performance, so the surrogate-based global sensitivity assessment is done based on WAS model in this section.

Table 3. Error estimates for different surrogate models.

	PRS	**KRG**	**RBNN**	**WAS**
Cavity length of range 1	16.49%	16.34%	17.88%	7.81%
ΔT_{max} of range 1	0.33%	13.66%	7.37%	0.15%

Fig. 5 evaluates the weights of each variable via global sensitivity analysis as pie-charts, as is illustrated in Fig. 5(a); C_l and L are exceedingly significant for cavity length, while ρ_v has less contribution, and C_v is the least influential parameter within the selected variations. Fig. 5(b) illustrates the percentage contribution of each variable for the maximum temperature drop ΔT_{max}; it can be observed that the weights of each variable are almost the same as that in Fig. 5(a). These observations indicate that thermodynamic effects play the dominant

Table 4. The range of the design variables based on case 1.

Variables	Range 1	Range 2
ρ_v	±10%	±13.52%
L	±10%	±1.08%
C_l	±10%	±0.5%
C_v	±10%	±1.27%
μ_l	/	±5.71%

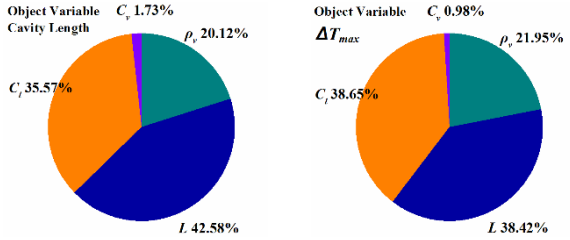

(a) The sensitivity of cavity length (b) The sensitivity of ΔTmax

Fig. 5. Pie-chart of global sensitivity analysis for chosen material properties with range 1.

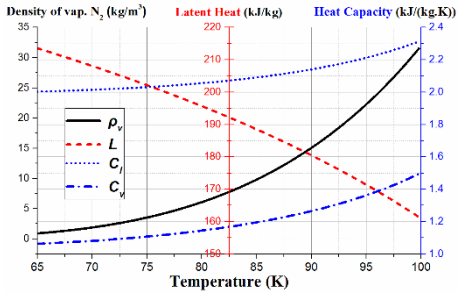

Fig. 6. Variation of physical properties for liquid nitrogen along saturation curve.

role in the cavitation dynamics when σ_∞ and R_e are kept as constant; the thermodynamic effects significantly affect flow structure and temperature distribution, which agrees with the result in Sec. 3.1. It also indicates the performance of thermodynamic effects on the current thermo-fluid cavitation numerical method is influenced by the properties in the mass transport equation as well as the energy equation.

The weights of each variable show that properties C_l, L and ρ_v have a significant influence on cavity structure; however, temperature-dependent properties vary differently with changing temperature. Fig. 6 illustrates the selected properties versus temperature; C_l, C_v and L change slowly with increasing temperature while ρ_v has higher slope of saturation curve with the increase of temperature, which means properties change differently when temperature is changing. According to the relative change ratio between each variable when liquid nitrogen temperature is at 83.06K, a new range of variables named range 2 is designed, as listed in Table 4: ρ_v changes considerably while another three variables change a little.

Fig. 7 evaluates the weights of each variable as pie-charts with the new range, which are completely different from range

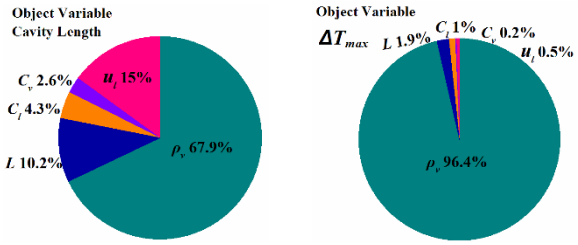

(a) The sensitivity of cavity length (b) The sensitivity of ΔTmax

Fig. 7. Pie-chart of global sensitivity analysis for chosen material properties with range 2.

1. For the cavity length, ρ_v accounts for 67.9%, L and μ_l affect the cavity structure slightly while C_l which significantly influences the cavity length in the range 1 as well as C_v could be ignored. It is observed that ρ_v plays the leading role on temperature drop, while L, C_l, C_v and μ_l do not have noticeable contribution, so the variation of these properties can be ignored when temperature is changing, and they can be kept as constant in thermo-fluid cavitating flows despite temperature may change obviously. When thermodynamic effects are taken into consideration in thermo-fluid cavitating flows, this method can be beneficial to select properties which should vary with temperature.

4. Conclusions

An effective numerical procedure coupled with energy equation is formulated for simulating thermo-fluid cavitating flows. The surrogate-based global sensitivity analysis is used to evaluate the effects of material thermophysical properties. The general conclusions of this paper are as follows.

(1) The thermal energy solution case yields a substantially shorter and mushier cavity attached on the hydrofoil due to the thermodynamic effects, which shows better agreement with the experimental measurements.

(2) The thermodynamic effects of the thermo-fluid cavitating flows significantly affect the cavitation dynamics, including pressure and temperature distribution, the variation of material thermophysical properties, and cavity structures. The temperature drop (evaporative cooling) inside the cavity decreases the local saturated vapor pressure and hence increases the local cavitation number, resulting in a smaller cavity, it could delay or suppress the occurrence and development of the cavitation behaviors.

(3) Thermodynamic parameter $\sum$ defined by material properties is shown to be critical in accurately predicting the intensity of thermodynamic effects on different fluids cavitating flows. The thermodynamic effects can be evaluated by thermophysical properties under the same free-stream conditions, becoming stronger with increasing temperature; strong thermodynamic effects could appear in hot water (T_∞= 437K) cavitating flow just as in cryogenic fluids.

(4) Among the primarily selected four properties, ρ_v, C_l and

L could significantly influence temperature drop (thermodynamic effects) and cavity structure in the existing numerical framework. The vapor density ρ_v plays the dominant role on temperature drop when these properties vary with changing temperature. The liquid viscosity μ_l slightly affects the flow structure via changing the Reynolds number R_e equivalently; however, it hardly affects the thermodynamic effects. This method is beneficial for selecting properties which should vary with temperature in thermo-fluid cavitating flow computation.

Thus, the study demonstrated that the Favre-averaged Navier-Stokes equations with the enthalpy-based energy equation are a powerful and reliable tool for understanding thermo-fluid cavitation behavior. As is known, the cavitation process is basically unsteady and there must be strong interactions between the cavity interface and the boundary layer during the cavitation development process. To further increase the accuracy of the predicted pressure and temperature fluctuations in the thermo-fluid cavitating flows, the thermodynamic effects as well as the unsteady characteristics should be considered in the numerical model in future work. Clearly, additional experimental and numerical studies are also needed to improve the understanding of the interaction between mass and heat transformation in the unsteady thermo-fluid cavitating flows.

Acknowledgment

This work was supported by the National Natural Science Foundation of China (NSFC, Grant Nos. 51479002 and 51306020).

Nomenclature

ρ : Density
V : Volume
L : Latent heat
C : Heat capacity
T : Temperature
ΔT^* : Nominal temperature drop
ΔT : Actual temperature drop
K : Thermal conductivity
σ : Cavitation number
p : Pressure
U : Velocity
t : Time
α : Volume fraction
μ : Dynamic viscosity
f : Mass volume fraction
h : Enthalpy
Pr : Prandtl number
$\sum$: Thermodynamic parameter
ε : Thermal diffusivity
Re : Reynolds number
$\dot{m}^+$: Condensation rate
$\dot{m}^-$: Evaporation rate
k : Turbulence kinetic energy

Subscripts

l : Liquid phase
v : Vapor phase
∞ : Reference
c : Critical point
m : Mixture
tur : Turbulent
lam : Laminar
i, j, k : Directions of the Cartesian coordinates

References

[1] G. Wang et al., Dynamics of attached turbulent cavitating flows, *Progress in Aerospace Sciences*, 37 (6) (2001) 551-581.
[2] E. Goncalvès and B. Charriere, Modelling for isothermal cavitation with a four-equation model, *International J. of Multiphase Flow,* 59 (2014) 54-72.
[3] B. Ji et al., Large eddy simulation and theoretical investigations of the transient cavitating vortical flow structure around a NACA66 hydrofoil, *International J. of Multiphase Flow*, 68 (2015) 121-134.
[4] S. Park and S. H. Rhee, Numerical analysis of the three-dimensional cloud cavitating flow around a twisted hydrofoil, *Fluid Dynamics Research*, 45 (1) (2013) 015502.
[5] B. Ji et al., Numerical analysis of unsteady cavitating turbulent flow and shedding horse-shoe vortex structure around a twisted hydrofoil, *International J. of Multiphase Flow*, 51 (2013) 33-43.
[6] B. Ji et al., Numerical simulation of three dimensional cavitation shedding dynamics with special emphasis on cavitation–vortex interaction, *Ocean Engineering*, 87 (2014) 64-77.
[7] G. Chen et al., Numerical study on the influence of interphase interaction in sheet/cloud cavitating flows around a 2D hydrofoil, *JMST*, 29 (3) (2015) 1075-1083.
[8] C. E. Brennen, *Cavitation and bubble dynamics*, Oxford University Press, New York, USA (1995).
[9] X. Tang et al., Numerical investigations on cavitating flows with thermodynamic effects in a diffuser-type centrifugal pump, *JMST*, 27 (6) (2013) 1655-1664.
[10] B. S. Kim, Y. K. Kim and J. Choi, Analysis of fluid induced vibration of cryogenic pipes in consideration of the cooling effect, *JMST*, 22 (12) (2008) 2375-2385.
[11] C. Lee and T. S. Roh, Flow instability due to cryogenic cavitation in the downstream of orifice, *JMST*, 23 (3) (2009) 643-649.
[12] H. A. Stahl and A. J. Stepanoff, Thermodynamic aspects of cavitation in centrifugal pumps, *ASME J. of Fluids Engineering*, 78 (1956) 1691-1693.
[13] J. P. Franc, C. Rebattet and A. Coulon, An experimental investigation of thermal effects in a cavitating inducer, *ASME J. of Fluids Engineering*, 126 (2004) 716-723.

[14] Y. Utturkar, J. Wu, G. Wang and W. Shyy, Recent progress in modeling of cryogenic cavitation for liquid rocket propulsion, *Progress in Aerospace Sciences*, 41 (7) (2005) 558-608.

[15] T. Goel, J. Zhao, S. Thakur, R. T. Haftka, W. Shyy and J. Zhao, Surrogate model based strategy for cryogenic cavitation model validation and sensitivity evaluation, *International J. for Numerical Methods in Fluids*, 58 (2008) 969-1007.

[16] E. W. Lemmon, M. O. McLinden and M. L. Huber, Reference fluid thermodynamic and transport properties, *NIST Standard Database 23*, version 7.0 (2002).

[17] J. Hord, Cavitation in liquid cryogens II-hydrofoils, *NASA*, CR-2156 (1973a).

[18] J. Hord. Cavitation in liquid cryogensIII-Ogives, *NASA*, CR-2242 (1973b).

[19] A. Hosangadi and V. Ahuja, A numerical study of cavitation in cryogenic fluids, *ASME J. of Fluids Engineering*, 127 (2005) 267-281.

[20] X. B. Zhang, L. M. Qiu, H. Qi, X. J. Zhang and Z. H.Gan, Modeling liquid hydrogen cavitating flow with the full cavitation model, *International J. of Hydrogen Energy*, 33 (2008) 7197-7206.

[21] B. Huang, Q. Wu and G. Wang, Numerical investigation of cavitating flow in liquid hydrogen, *International J. of Hydrogen Energy*, 39 (4) (2014) 1698-1709.

[22] J. Zhu et al., Extension of the Schnerr–Sauer model for cryogenic cavitation, *European J. of Mechanics-B/Fluid*, 52 (2015) 1-10.

[23] Z. Yao et al., A thermodynamic cavitation model for cavitating flow simulation in a wide range of water temperatures, *Chinese Physics Letters*, 27 (1) (2010) 016401.

[24] C. Tseng and W. Shyy, Surrogate-based modeling of cryogenic turbulent cavitating flows, *Proc. of CAV2009 the 7th International Symposium on Cavitation*, Ann Arbor, MI, USA (2009) 17-22.

[25] M. Murakami and K. Harada, Experimental study of thermo-fluid dynamic effect in He II cavitating flow, *Cryogenics*, 52 (2012) 620-628.

[26] Y. Yoshida et al., Thermodynamic effect on rotating cavitation in an inducer, *ASME J. of Fluids Engineering*, 131 (9) (2009) 091302-7.

[27] F. R. Menter, Improved two-equation k-ω turbulence models for aerodynamic flows, *NASA Technical Memorandum*, 3t (1992) 103975.

[28] I. Senocak and W. Shyy, Interfacial dynamics-based modeling of turbulent cavitating flows, Part-1: model development and steady-state computations, *International J. for Numerical Methods in Fluids*, 44 (2004) 975-995.

[29] C. L. Merkle, J. Feng and P. E. O. Buelow, Computational modeling of dynamics of sheet cavitation, *Proc.of Cav1998 the 3rd International Symposium on Cavitation*, Grenoble, France (1998) 307-311.

[30] Y. Utturkar, Computational modeling of thermodynamic effects in cryogenic cavitation, *Ph.D. Dissertation*, University of Florida (2005).

[31] S. Shi and G. Wang, Numerical calculation of thermal effect on cavitation in cryogenic fluids, *Chinese J. of Mechanical Engineering*, 25 (6) (2012) 1176-1183.

[32] M. M. Athavale et al., Application of the full cavitation model to pumps and inducers, *International J. of Rotating Machinery*, 8 (1) (2002) 45-56.

[33] C. Tseng and W. Shyy, Turbulence modeling for isothermal and cryogenic cavitation, *Proc.of 47th AIAA Aerospace Science Meeting*, Orlando, FL AIAA Paper No. 2009-1150 (2009).

[34] C. Tseng, Y. Wei, G. Wang and W. Shyy, Modeling of turbulent, isothermal and cryogenic cavitation under attached conditions, *Acta Mechanica Sinica*, 26 (2010) 325-353.

[35] A. Yu et al., Cavitation simulation with consideration of viscous Effect at Large Liquid Temperature Variation, *Chinese Physics Letters*, 31 (8) (2014) 086401.

[36] R. H. Myers and D. C. Montgomery, *Response surface methodology*, John Wiley & Sons (1995).

[37] M. D. McKay, R. J. Beckman and W. J. Conover, A comparison of three methods of selecting values of input variables in the analysis of output from a computer code, *Technometrics*, 21 (1979) 239-245.

[38] G. Matheron, Principles of geostatistics, *Economic Geology*, 58 (1963) 1246-1266.

[39] M. J. L. Orr, Introduction to radial basis function networks, *Center for Cognitive Science*, Edinburgh University, EH 9LW, Scotland, UK (1996).

[40] T. Goel, R. T. Haftka, W. Shyy and N. V. Queipo, Ensemble of surrogates, *J. of Structural and Multidisciplinary Optimization*, 33 (3) (2007) 199-216.

Tairan Chen received his B.S. from Beijing Institute of Technology, Beijing, China in 2013. He is a doctoral student in Mechanical Engineering School of Beijing Institute of Technology, majoring in fluid dynamics. His research field includes experimental study on cryogenic cavitation and computations of multiphase flows. He is involved in thermal-hydrodynamics of cavitating flows.